

A local correlation-based zero-equation transition model

Jatinder Pal Singh Sandhu*, Santanu Ghosh

Department of Aerospace Engineering, IIT Madras, Chennai, India

ARTICLE INFO

Article history:

Received 25 January 2020

Revised 19 August 2020

Accepted 7 September 2020

Available online 6 October 2020

Keywords:

Laminar to turbulent transition

Zero-equation

Local correlation-based transition model

ABSTRACT

In this work, the local correlation-based one-equation transition model (Menter, F.R., Smirnov, P.E., Liu, T. and Avancha, R., A one-equation local correlation-based transition model. *Flow, Turbulence and Combustion*, vol. 95, no. 4, pp. 583–619, 2015.) is transformed into a zero-equation transition model. The new model provides an attractive choice in terms of quick implementation of a transition model in existing turbulent flow solvers with Menter's shear-stress transport (SST) turbulence model, as it only introduces three extra source terms in the transport equation of turbulent kinetic energy. The model is validated against a set of benchmark flat-plate test cases: T3 series and SK, and also subsonic flows past two different airfoils: Aerospatiale A-airfoil ($Re = 2.1$ million) and E387 ($Re = 0.2$ million), and finally applied to a transonic flow over 3D DLR-F5 wing ($Re = 1.5$ million). Results show that the proposed model produces similar transition prediction as the one-equation transition model, with a reduced computational effort. The computations are performed with an in-house finite-volume solver for compressible turbulent flows on block-structured grids.

© 2020 Elsevier Ltd. All rights reserved.

1. Introduction

Laminar-to-turbulent transition is a complex phenomenon affected by a large number of parameters like free-stream turbulence intensity, pressure gradient, Reynolds number, Mach number, surface temperature, etc. [1–5]. This wide range of parameters lead to different types of transition mechanisms: natural transition[6], bypass transition[7], cross-flow transition [8], etc. As such, it is challenging for single-physics based transition models, like the e^N linear stability theory [9,10] for natural transition, the low Reynolds number turbulence model [11] for bypass transition, to predict all the different paths to transition. Although LES (Large Eddy Simulation) and DNS (Direct Numerical Simulation) [12,13] are suitable for transition prediction, the amount of computational memory required and time consumed for even a simple geometry is large.

The experimental correlation-based transition models [1,14–18] provide a unified concept, which can handle the different transition mechanisms, but suffers from one major issue: compatibility with modern-day code and computer architecture due to the use of integral boundary layer parameter. There are certain features of modern-day CFD codes that impose few restrictions on the model formulation, detailed in Langtry and Menter [19]. M. Lorini et al. [20] have tried to bypass the compatibility issue in their finite-element method by defining a wall-normal integral cell line and

making sure that this line is not decomposed into separate domains by using a specialized domain partitioning procedure. However, it remains to be seen if this approach will work for a complex domain. Menter et al.[21] presented an idea to remedy the shortcoming of the correlation-based transition model by replacing the integral parameter used in the model, Re_θ , with local parameter Re_v , based on the relation presented first in Blumer and Van Driest [22] (shown in Eq. (1)) and termed it Local Correlation-based Transition Modeling (LCTM). Fig. 1 shows the variation of scaled Re_v within the boundary layer for the Blasius profile. The quantity Re_v reaches a maximum value in the middle of the boundary layer.

$$Re_\theta = \frac{\max(Re_v)}{2.193} \quad (1)$$

where,

$$Re_v = \frac{\rho y^2}{\mu} S \quad (2)$$

where, y is wall-distance and S is the absolute value of strain rate, $(2S_{ij}S_{ij})^{1/2}$. The two-equation $\gamma - Re_\theta$ model was developed based on the LCTM concept [3,19,23–26], but the model was not Galilean invariant and contained complex correlations. The successor of the $\gamma - Re_\theta$ model, the one-equation γ model [27], removed some of the shortcomings of its predecessor, and reduced the model's complexity. The single intermittency (γ) transport equation based transition models were also proposed in Coder and Maughmer [28], Ge et al. [29]. Bas et al. [30,31] went a step further by replacing the transport equation of the transition variable

* Corresponding author.

E-mail address: ae15d400@smail.iitm.ac.in (J.P.S. Sandhu).

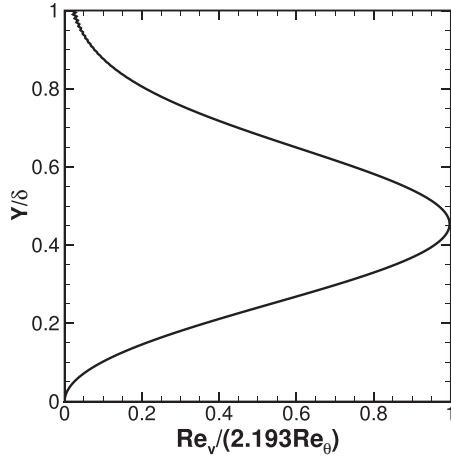


Fig. 1. Profile of scaled strain-rate Reynolds number in a Blasius boundary layer.

with a function for intermittency, creating an algebraic transition model (“BC” transition model) and integrated it with the Spalart Allmaras (SA) [32] turbulence model. The intermittency function in “BC” algebraic transition model controls the production term in the SA model to predict the laminar to turbulence transition. The BC transition model is, however, not Galilean invariant and utilizes the freestream turbulence intensity, as opposed to the local turbulence intensity, in the correlation for transition prediction. The BC transition model also depends on the flow Reynolds number and requires modification in the inlet conditions of the original SA turbulence model.

Apart from the local correlation-based transition models, there are laminar-kinetic-energy based transition models. These models are based on the shear-sheltering concept [33] and solve a separate transport equation of laminar kinetic energy or a similar quantity [34–36] and even add a second transport equation of intermittency [37]. Recently, Kubacki et al. proposed an algebraic laminar-turbulent transition model based on the same concept for bypass transition in turbomachinery flows [38]. They further extended the model’s capability for separation-induced and wake-induced transition [39]. Interestingly, Mishra et al. [40] were able to predict the laminar-separation-bubble induced transition by just introducing the non-linear corrections to the SST turbulence model.

In this work, we propose a new local correlation-based zero-equation transition model, which can predict transition due to causes (natural, bypass, or separation induced) for which correlations are formulated. Inspired by work done for the development of one-equation turbulence model [41], the local correlation-based one-equation γ transition model [27], combined with the two-equation $k - \omega/k - \epsilon$ SST2003 [42] turbulence model is transformed into a zero-equation LCTM by defining a new variable: k_γ as

$$k_\gamma = \gamma k \quad (3)$$

where γ is the intermittency and k is the turbulent kinetic energy. In the fully turbulent boundary layer, the k_γ variable physically represents turbulent kinetic energy k . Although we derive the transport equation of the newly defined k_γ variable from the transport equations of k and γ , the final form of the model essentially solves the transport equation of turbulent kinetic energy (k), similar to the SST turbulence model, with few additional source terms that give it the ability to predict transition. As such, the new model, in its entirety, can also be thought of as a two-equation turbulence-transition model. Although the new formulation does not try to reduce the complexity of the underlying one-equation γ transition model, it reduces the complexity of its implementa-

tion (related to construction of Jacobian matrices for fully implicit time integration of discretized equations) by reducing the number of transport equations to be solved for the combined turbulence/transition model.¹ As the proposed model introduces a new variable k_γ , it is named as the k_γ transition model.

The outline of the rest of the paper is as follows. Section 2 provides the details of the flow solver utilized for the current study, and the detailed model formulation of the new k_γ transition model. Section 3 presents the validation of the new transition model along with its comparison with the one-equation γ transition model for a set of benchmark flat-plate test cases: Schaubauer and Klebanoff (SK) test case [43], and T3 series test cases [44]. The capability of the new k_γ transition model to predict transition is also tested for two different airfoils: Aerospatiale A [45] and Eppler 387 airfoil [46], and a 3D test case: DLR-F5 wing [47].

2. Methodology

2.1. Flow solver

All the numerical simulations presented here are performed using an in-house finite volume solver, FEST-3D [48,49]. It solves the compressible-flow based three-dimensional, Favre-averaged [50], Navier-Stokes equations on a structured grid. Governing equations used in FEST-3D are of the following form:

$$\begin{aligned} \frac{\partial \rho}{\partial t} + \frac{\partial}{\partial x_j} (\rho u_j) &= 0 \quad (4) \\ \frac{\partial (\rho u_i)}{\partial t} + \frac{\partial}{\partial x_j} (u_j \rho u_i) &= -\frac{\partial p}{\partial x_i} + \frac{\partial}{\partial x_j} \left(2\mu_{eff} \left(S_{ij} - \frac{1}{3} \frac{\partial u_k}{\partial x_k} \delta_{ij} \right) - \frac{2}{3} \rho k \delta_{ij} \right) \\ \frac{\partial (\rho E)}{\partial t} + \frac{\partial}{\partial x_j} (u_j \rho H) &= \frac{\partial}{\partial x_j} \left(2\mu_{eff} \left(S_{ij} - \frac{1}{3} \frac{\partial u_k}{\partial x_k} \delta_{ij} \right) - \frac{2}{3} \rho k \delta_{ij} \right) u_i \\ &\quad + \frac{\partial}{\partial x_j} \left(\left(\frac{c_p \hat{\mu}}{Pr} + \frac{c_p \hat{\mu}_t}{Pr_t} \right) \frac{\partial T}{\partial x_j} + \left(\mu + \frac{\mu_t}{\sigma_k} \right) \frac{\partial k}{\partial x_j} \right) \end{aligned}$$

where, ρ is density, and u_i is local velocity. The total enthalpy, H , is given by:

$$H = E + p/\rho \quad (5)$$

E being the total internal energy. In FEST-3D, there is an option to use either constant viscosity or use Sutherland’s law to determine the local value of dynamic viscosity using the local temperature, T as

$$\mu = \mu_0 \left(\frac{T}{T_0} \right)^{3/2} \left(\frac{T_0 + T_S}{T + T_S} \right) \quad (6)$$

where $\mu_0 = 1.716 \times 10^{-5}$ kg/(ms), $T_0 = 273.15$ K, and $T_S = 110.4$ K. The effective viscosity μ_{eff} is a sum of turbulent viscosity (μ_t) and molecular viscosity (μ). The expression for turbulent viscosity depends on the turbulence model being used. For SST2003 turbulence model used in this study, μ_t is evaluated as:

$$\mu_t = \frac{\rho a_1 k}{\max(a_1 \omega, F_2 S)} \quad (7)$$

where, k is turbulent kinetic energy, ω is specific turbulence dissipation rate, S is the absolute value of strain rate, and Ω is absolute value of vorticity. The reader can refer to [42] for the constant a_1 and blending function F_2 .

FEST-3D provides several options in terms of turbulence models, high-resolution methods for face-state reconstruction, inviscid flux reconstruction, and time-integration, details of which can be found in Singh Sandhu et al. [48]. The current work utilizes the

¹ The reduction in the number of equations also reduces the memory requirement and computational cost per iteration.

3rd order accurate MUSCL [51] scheme as the face-state reconstruction method, AUSM+UP [52] as the inviscid flux reconstruction method and matrix-free LU-SGS [53] as the implicit time-integration method. For low Mach number flow, preconditioning [54] is applied to the LU-SGS scheme to obtain better convergence. Such choice of flux reconstruction and time-integration scheme is motivated by the work of Kitamura et al. [55].

2.2. k_γ transition model

The formulation of the k_γ transition model is described in this section. The transport equation for k_γ is first derived, and then new terms appearing in the equation are modeled.

In order to formulate the zero-equation transition model, the unsteady transport of the term k_γ is expressed in terms of the unsteady transport of turbulent kinetic energy and intermittency. Thus,

$$\begin{aligned} \frac{\partial \rho k_\gamma}{\partial t} + \frac{\partial u_j \rho k_\gamma}{\partial x_j} &= \frac{\partial \rho \gamma k}{\partial t} + \frac{\partial u_j \rho \gamma k}{\partial x_j} \\ &= \gamma \left(\frac{\partial \rho k}{\partial t} + \frac{\partial u_j \rho k}{\partial x_j} \right) + k \left(\rho \frac{\partial \gamma}{\partial t} + \rho u_j \frac{\partial \gamma}{\partial x_j} \right) \\ &= \gamma \left(\frac{\partial \rho k}{\partial t} + \frac{\partial u_j \rho k}{\partial x_j} \right) + k \left(\frac{\partial \rho \gamma}{\partial t} + \frac{\partial u_j \rho \gamma}{\partial x_j} \right) \\ &\quad - \gamma k \left(\frac{\partial \rho}{\partial t} + \frac{\partial u_j \rho}{\partial x_j} \right) \end{aligned}$$

Since from continuity equation, $\frac{\partial \rho}{\partial t} + \frac{\partial u_j \rho}{\partial x_j} = 0$, this implies:

$$\frac{\partial \rho k_\gamma}{\partial t} + \frac{\partial u_j \rho k_\gamma}{\partial x_j} = \gamma \left(\frac{\partial \rho k}{\partial t} + \frac{\partial u_j \rho k}{\partial x_j} \right) + k \left(\frac{\partial \rho \gamma}{\partial t} + \frac{\partial u_j \rho \gamma}{\partial x_j} \right) \quad (8)$$

In Eq. (8), the right hand side contains the unsteady transport terms of ρk and $\rho \gamma$ and need to be replaced with the source and diffusion terms from the corresponding transport equations. In order to keep the discussion brief, the original transport equations of k and γ are not presented here and one can refer to [27] for details of the terms used in following equation:

$$\begin{aligned} \frac{\partial \rho k_\gamma}{\partial t} + \frac{\partial u_j \rho k_\gamma}{\partial x_j} &= \gamma \left(P_k + P_k^{lim} - E_k + \frac{\partial}{\partial x_j} \left[(\mu + \sigma_k \mu_t) \frac{\partial k}{\partial x_j} \right] \right) \\ &\quad + k \left(P_\gamma - E_\gamma + \frac{\partial}{\partial x_j} \left[(\mu + \sigma_\gamma \mu_t) \frac{\partial \gamma}{\partial x_j} \right] \right) \end{aligned} \quad (9)$$

Here, P_ϕ , E_ϕ , D_ϕ represent the production, destruction, and diffusion terms in the transport equation of the variable $\phi \in \{k, \gamma\}$ respectively. The terms σ_k and σ_γ are the diffusion coefficients for k and γ variables respectively. To keep the derivation simple and reproduce the behavior of the SST model in the fully turbulent flow, the following assumption is made here:

$$\sigma_\gamma = \sigma_k \quad (10)$$

Now, using Eq. (10), the Eq. (9) can be rewritten as:

$$\frac{\partial \rho k_\gamma}{\partial t} + \frac{\partial u_j \rho k_\gamma}{\partial x_j} = P_{k_\gamma}^{(k)} + P_{k_\gamma}^{lim} - E_{k_\gamma}^{(k)} + D_{k_\gamma}^{(k)} + P_{k_\gamma}^{(\gamma)} - E_{k_\gamma}^{(\gamma)} + D_{k_\gamma}^{(\gamma)} \quad (11)$$

where the derivation of each source and diffusion term is detailed in Appendix A. The source and diffusion terms which are similar in appearance to those in the original k transport equation are given the superscript (k) and others the superscript (γ) respectively.

In order to interpret the transport equation of k_γ as that of k in Eq. (11), the definition of k_γ variable is invoked in the different

parts of the boundary layer. Since intermittency is zero in the laminar flow region and unity in the fully turbulent flow region, k_γ can be written as a piece-wise function.

$$k_\gamma = \begin{cases} k = 0, & \text{in the laminar boundary layer} \\ k_\gamma, & \text{in the transition flow region} \\ k, & \text{in the fully turbulent flow region} \end{cases} \quad (12)$$

As seen in literature [31,38], the length of transition region predicted by the zero-equation/algebraic transition models is very short. Thus, we do not consider the transition region for modeling, and we replace the k_γ variable in Eq. (11) with k .

$$k_\gamma = k \quad (13)$$

Hence, the transport equation of k_γ is written as a transport equation of k as:

$$\frac{D\rho k}{Dt} + \rho k \frac{\partial u_j}{\partial x_j} = P_k + P_k^{lim} - E_k + \frac{\partial}{\partial x_j} \left[(\mu + \sigma_k \mu_t) \frac{\partial k}{\partial x_j} \right] + \Psi_{k_\gamma} \quad (14)$$

where,

$$\Psi_{k_\gamma} = P_k^{(\gamma)} - E_k^{(\gamma)} + D_k^{(\gamma)} \quad (15)$$

In doing so, we are able to incorporate the effect of γ transport equation into the transport equation of k with the additional source terms: Ψ_{k_γ} , to predict transition directly. A point to note about Eq. (14) is that it contains terms with the variable intermittency, which is not known and needs to be approximated. We choose to approximate the unknown intermittency in Eq. (14) such that it introduces the required near-wall viscous damping effect. There are different ways to estimate the intermittency to produce this effect. In this study, we follow the viscous damping function used in Walters and Cokljat [34], and estimate intermittency ($\tilde{\gamma}$) using turbulent Reynolds number (R_T) as:

$$\gamma \approx \tilde{\gamma} = (1 - e^{-R_T})^n \quad (16)$$

and,

$$\frac{\partial \tilde{\gamma}}{\partial x_i} = \frac{n \rho \tilde{\gamma}^{(n-1)/n}}{\mu \omega} \left(\frac{\partial k}{\partial x_i} - \frac{k}{\omega} \frac{\partial \omega}{\partial x_i} \right) e^{-R_T} \quad (17)$$

where,

$$R_T = \frac{\rho k}{\omega \mu} \quad (18)$$

In order to obtain the gradient of $\tilde{\gamma}$ in Eq. (17), the gradient of density (ρ) and molecular viscosity (μ) have been ignored.

A point to note about the modeling of γ is that although the use of R_T in $\tilde{\gamma}$ is an obvious choice, it makes the model sensitive to initial conditions for low freestream turbulence intensity cases, as shown in Appendix B. This shortcoming may potentially be removed by introducing a different approximation for $\tilde{\gamma}$ (which is both accurate and is not sensitive to initial conditions). The current form of the k_γ model is calibrated for freestream initial conditions. Additionally, unlike the intermittency used in Cakmakcioglu et al. [31], Kubacki and Dick [38], the approximated intermittency $\tilde{\gamma}$ itself can not predict transition in the present framework, and relies on F_{onset} to trigger transition.

Fig. 2 shows the variation of the estimated intermittency ($\tilde{\gamma}$) in the wall-normal direction for SK flat plate test case [43] in the fully turbulent and laminar flow region. The wall-normal distance is normalized with boundary layer thickness (δ). The constant 'n' in Eq. (16) is calibrated such that the estimated intermittency is zero in laminar region and matches with γ from one-equation transition model in the fully turbulent region. From Fig. 2a it can be

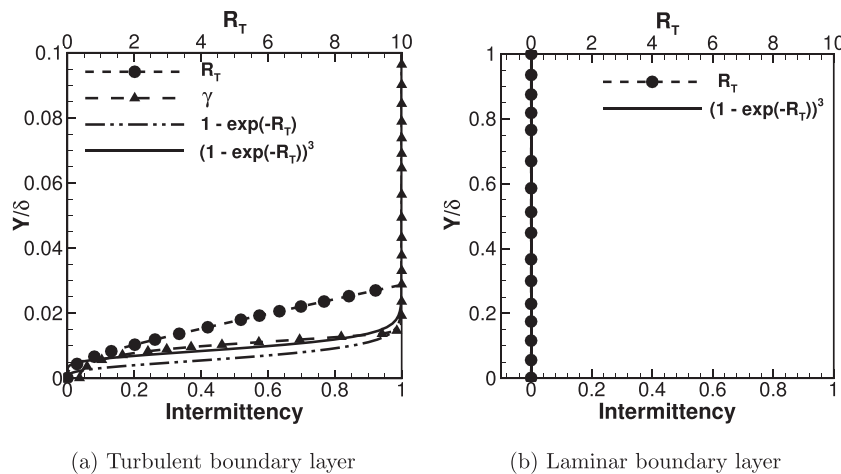


Fig. 2. Comparison of intermittency and its approximation for the SK test case in (a) turbulent flow at $Re_x = 519885$, and (b) laminar flow at $Re_x = 50841$.

observed that when $n = 3$, the estimated intermittency ($\tilde{\gamma}$), represented by the solid line, is close to the intermittency (γ), represented by the dashed line, obtained using the one-equation transition model. In the laminar region, the quantity R_T (Eq. (18)) vanishes quickly from its freestream value as one approaches the wall. Hence, $\tilde{\gamma}$, represented by the solid line, has a zero value in the laminar boundary layer, as shown in Fig. 2b.

Using the estimated intermittency ($\tilde{\gamma}$), all the source terms in Eq. (14) are defined as:

$$P_k = \tilde{\gamma} \mu_t S \Omega = \frac{\tilde{\gamma} \rho a_1 k}{\max(a_1 \omega, S F_2)} S \Omega \quad (19)$$

$$E_k = \max(\tilde{\gamma}, 0.1) \beta^* \rho \omega k \quad (20)$$

$$P_k^{(\gamma)} = F_{length} \rho S (1 - \tilde{\gamma}) F_{onset} k \quad (21)$$

$$E_k^{(\gamma)} = \tilde{\gamma} C_{e1} \rho \Omega F_{turb} k \quad (22)$$

$$D_k^{(\gamma)} = -C_{d1} \mu_{eff} \frac{\partial k}{\partial x_j} \frac{\partial \tilde{\gamma}}{\partial x_j} \quad (23)$$

Here,

$$F_{turb} = e^{-\left(\frac{R_T}{2}\right)^4} \quad (24)$$

and the onset of transition is controlled by the following function:

$$F_{onset} = \max(F_{onset2} - F_{onset3}, 0.0) \quad (25)$$

where,

$$F_{onset2} = \min(F_{onset1}, 2.0) \quad (26)$$

and

$$F_{onset3} = \max\left(1 - \left(\frac{R_T}{3.5}\right)^3, 0\right) \quad (27)$$

In Eq. (26), the term F_{onset1} is defined as,

$$F_{onset1} = \frac{Re_\nu}{2.2 Re_{\theta c}} \quad (28)$$

Also, $Re_{\theta c}$ is calculated using the following correlation:

$$Re_{\theta c} = 100.0 + 1000.0 \exp(-Tu_L F_{PG}) \quad (29)$$

Here, the terms Tu_L and F_{PG} are functions that account for the effects of local turbulence intensity and pressure gradient in the flow. They are defined as:

$$F_{PG} = \begin{cases} \min(1 + 14.68 \lambda_{\theta L}, 1.5), & \lambda_{\theta L} \geq 0 \\ \min(1 - 7.34 \lambda_{\theta L}, 3.0), & \lambda_{\theta L} < 0 \end{cases} \quad (30)$$

and

$$Tu_L = \min\left(100 \frac{\sqrt{2k/3}}{\omega d_w}, 100\right) \quad (31)$$

Here, d_w is the wall distance. The pressure gradient parameter, $\lambda_{\theta L}$, is defined as

$$\lambda_{\theta L} = -7.57 \cdot 10^{-3} \frac{dV}{dy} \frac{d_w^2}{v} + 0.0128 \quad (32)$$

The term $\frac{dV}{dy}$ can be computed as:

$$\frac{dV}{dy} = \nabla(\vec{n} \cdot \vec{V}) \cdot \vec{n} \quad (33)$$

where,

$$\vec{n} = \frac{\nabla(d_w)}{|\nabla(d_w)|} \quad (34)$$

The results for the T3C2 flat plate test case: evolution of skin friction coefficient (C_f) along the length of plate ($Re_x = \rho U_{inf} x / \mu$) and contours of normalized (with freestream speed of sound, a_{ref}) k_γ , using the k_γ model, are shown in Fig. 3. It can be seen from Fig. 3a that the k_γ model predicts early transition in this case. This is corroborated in Fig. 3b wherein it can be observed that normalized k_γ reaches high values close to the leading edge of the plate. In Fig. 3b, 'X' is along the length of the plate, and 'Y' in the wall-normal direction, and approximate edge of the boundary layer is shown with a white line.

The reason for this early prediction of transition was determined to be the following: with the original F_{length} from [27], the order of the production terms arising from the transport equation of intermittency, $P_k^{(\gamma)}$, is about $100(\gamma - 1)/\gamma$ times higher than its counterpart P_k , so that even a small value of F_{onset} function can trigger a permanent transition. As such, a modification to the k_γ model was made by reducing the F_{length} to be unity, and tuning the other coefficients accordingly. The final values of the coefficients used are listed in Eq. (35).

$$F_{length} = 1 \quad (35a)$$

$$C_{e1} = 0.03 \quad (35b)$$

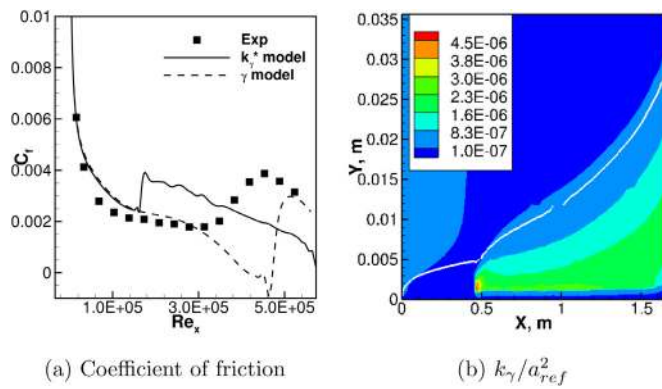


Fig. 3. Results for the T3C2 test case with the original model constants: $F_{length} = 100$, $C_{e1} = 3$, and $C_{d1} = 2$.

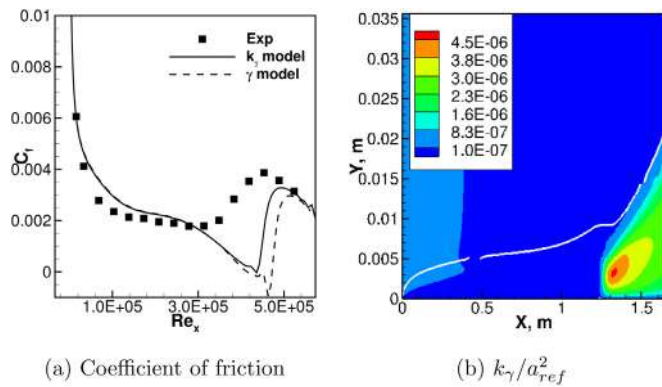


Fig. 4. Results for the T3C2 test case with the modified model constants: $F_{length} = 1$, $C_{e1} = 0.03$, and $C_{d1} = 0.02$.

Table 1
Inlet conditions for flat plate test cases.

Case	U[m/s]	Tu(%)	μ_t/μ	$Re_\infty(L_{Ref} = 1\text{ m})$
T3A	5.20	3.5	12	3.5×10^5
T3B	9.40	6.2	100	6.3×10^5
T3A-	19.80	1.0	8	1.4×10^6
S&K	50.10	0.03	1	3.4×10^6
T3C1	6.10	7.0	60	4.1×10^5
T3C2	5.25	3.1	9	3.5×10^5
T3C3	3.90	3.1	6	2.6×10^5
T3C5	8.90	3.8	15	5.9×10^5

$$C_{d1} = 0.02 \tag{35c}$$

The evolution of the skin friction coefficient and contours of normalized k_γ (with the edge of the boundary layer represented by white line) with the new set of coefficients are again plotted in Fig. 4. As can be seen in Fig. 4, this results in much better prediction of transition. Contours of normalized k_γ reveal that in this case, the transition location has been pushed down to about 1.25 m from the leading edge of the plate.

3. Validation

The k_γ model is validated against a set of common benchmark test cases for transition modeling: the ERCOFTAC (European Research Community on Flow, Turbulence, and Combustion) T3 series of experimental flat plate test cases [44], which are listed in Table 1. The experimental setup consisted of a flat plate of 1.5 m of length with a rounded leading edge of 0.75 mm radius mounted

in a wind-tunnel test section. The T3A, T3B, and T3A- test cases were performed with zero pressure gradient and 3.0, 6.0 and 1.0% freestream turbulence intensity respectively, which makes bypass as the dominant transition mechanism. The Schubauer and Klebanoff (S&K) flat plate experiment [43], performed in relatively quiet wind tunnel conditions with a freestream turbulence intensity of 0.03%, is used here to validate the k_γ model's prediction of natural transition mechanism. The rest of the T3 series test cases were performed with a high free-stream turbulence intensity, as listed in Table 1, and a streamwise pressure gradient was imposed due to the convergent-divergent upper wall of the wind tunnel.

3.1. Computational details

For all the validation simulations, air is assumed as the working fluid with freestream density of $\rho = 1.2 \text{ kg/m}^3$ and constant viscosity of $\mu = 1.8 \times 10^{-5} \text{ kg/m}\cdot\text{s}$. To obtain better convergence for low-speed validation test cases, AUSM+-UP [52] is used as the flux-reconstruction scheme with preconditioned [54] LU-SGS as the time integration method for all the validation simulations. The inlet conditions for these test cases are given in Table 1. The inlet turbulent kinetic energy and viscosity ratio, listed in Table 1, are determined via trial and error such that the decay of freestream turbulent kinetic energy in the simulation matches with experimental data [44].

For S&K and T3 series flat plate test cases without pressure gradient (T3A, T3B, and T3A-), a similar rectangular domain with a structured grid, clustered near the leading edge, is used, as shown in Fig. 5a. The computational domain consists of a 1.5 m long horizontal, adiabatic, no-slip flat plate with a vertical inlet plane located at a short distance of 0.04 m ahead of the leading edge of the plate, which allows the prescription of uniform velocity and density at the inlet. The inviscid region between the leading edge and inlet plane is kept short as experimental data [44] does not contain any information about the flow ahead of the leading edge of the plate. The horizontal top boundary at 0.8 m above the flat plate was treated with symmetry boundary condition. At the vertical outflow plane, a pressure of 103320 Pa is imposed.

For the flat plate test cases with a pressure gradient, the computational domain (shown in Fig. 5b) consisted of a 1.65 m long horizontal, adiabatic, no-slip flat plate with vertical inlet plane situated at 0.1 m ahead of the leading edge of the plate. The boundary conditions at the inlet and outlet planes are the same as in the zero pressure gradient test cases. The contour of the upper slip wall is obtained from the explicit expression given in [56]. The distance between the upper and lower wall is 0.3 m at the inlet plate. The profile of the upper wall and comparison of predicted normalized freestream velocity with experiment [44] having the same upper-wall profile is shown in Fig. 6.

3.2. Grid convergence study

A grid refinement study is performed to ensure grid independence of the solution for the flat plate test cases. Grids are generated using the meshing guidelines provided in Menter et al. [27] for the one-equation γ transition model, which ensures that the same grid can be employed to make a comparison between k_γ and γ transition models. Four different grid levels are used for the study: "Level 0", "Level 1", "Level 2" and "Level 3" for both zero pressure gradient and pressure gradient test cases, wherein "Level 0" is the finest and "Level 3" is the coarsest mesh. The "Level 1" grid is obtained from "Level 0" grid by removing every alternate point in both streamwise and wall-normal direction. Similarly, the "Level 2" and "Level 3" grids are obtained using the same approach from the "Level 1" and "Level 2" grids respectively. Details about the grid dimensions and number of points on the plate at each

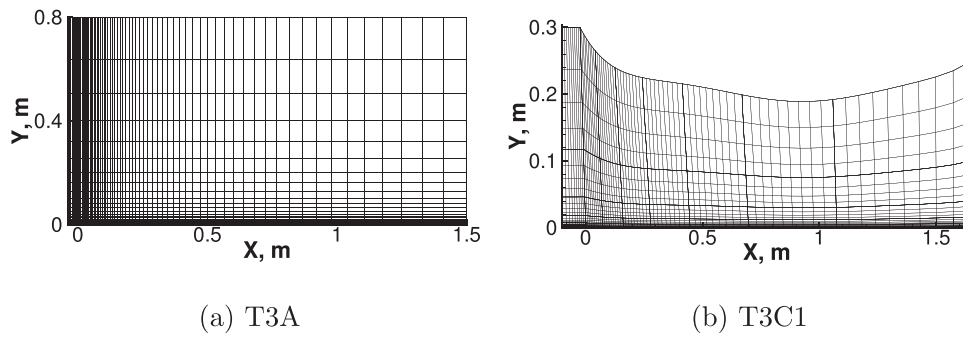


Fig. 5. Level 3 grid used for convergence study of flat plate test cases.

Table 2
Grid details.

Grid level	Zero pressure gradient	Non-zero pressure gradient	Points on the plate
Level 0	569 × 321	577 × 257	505
Level 1	285 × 161	289 × 129	253
Level 2	143 × 81	145 × 65	127
Level 3	72 × 41	73 × 33	64

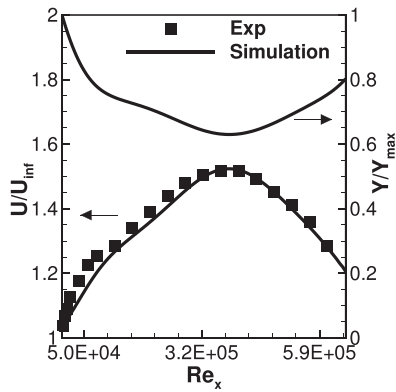


Fig. 6. The profile of the upper wall and its effect on freestream velocity for pressure gradient flat plate test cases, compared with experiment [44].

grid level are listed in Table 2. As evident from Fig. 7, the “Level 0” and “Level 1” grids give almost overlapping results in terms of the coefficient of friction along the flat plate for T3A, SK, and T3C5 test cases. As such, “Level 1” grid is used for validation purposes.

The distance of the first grid point in the wall-normal direction for “Level 1” grid is chosen such that a y^+ value of less than one is maintained over the turbulent region on the flat plate. The same grid (“Level 1”) is used for T3A, T3B and T3A- test cases and the

grid has the first grid point at a distance of 10^{-5} m in the wall-normal direction. For the SK test case, the first wall-normal grid point is situated at a distance of 2.5×10^{-6} m from the plate. For all the pressure gradient flat plate test cases, the first grid point is located at a wall-normal distance of 2×10^{-5} m from the plate. Further, in all the flat plate test cases, the grid is clustered near the leading edge with the first grid point 10^{-3} m away from the leading edge in the streamwise direction.

3.3. Results

The inlet turbulence intensity and viscosity ratio used in the current study are similar to those used in Menter et al. [27]. The procedure adopted in determining the used values of turbulent intensity and viscosity ratio at inlet is as described in Langtry and Menter [19], wherein the inlet turbulence intensity was fixed and, via trial and error, the viscosity ratio was adjusted to match the experimentally measured turbulence levels [44] at various downstream locations. Fig. 8 shows the comparison of the variation of free-stream turbulence intensity (Tu in percentage) with experimental data [44] along the length of a plate for the flat plate test cases. Since similar experimental data for the SK test case is not available, the same is not included in Fig. 8. Although these results, marked as simulation, are shown for the k_γ model, identical results were obtained for γ model.

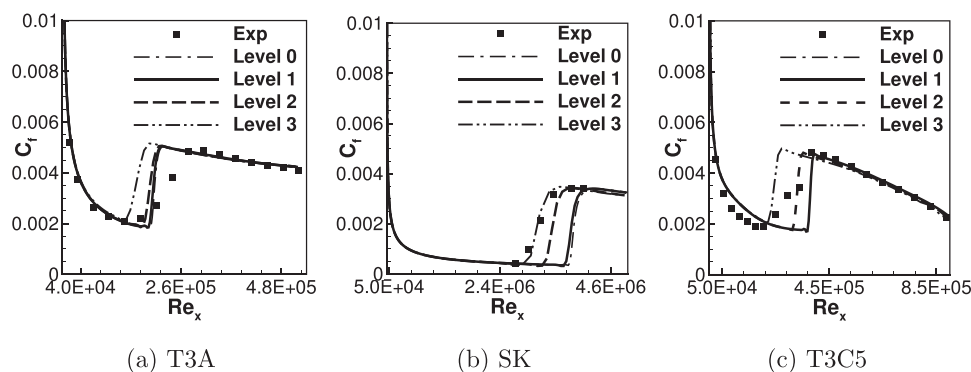


Fig. 7. Grid-convergence study for flat plate test cases.

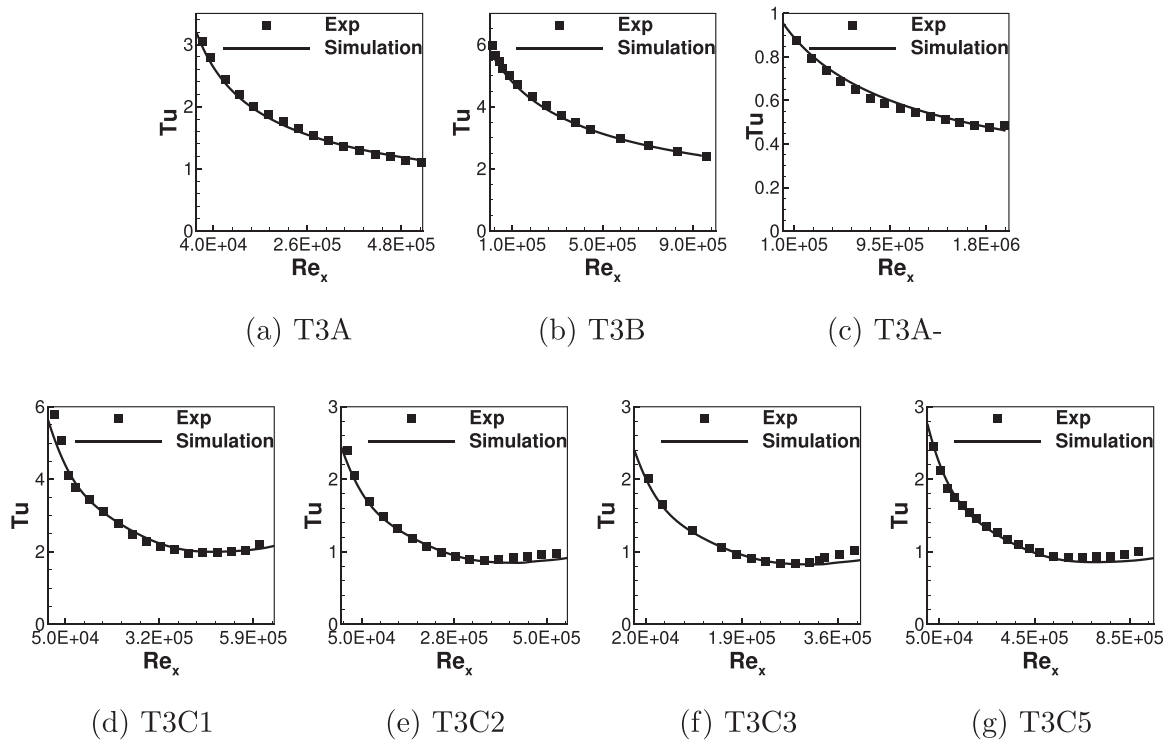


Fig. 8. Free-stream turbulence intensity versus local Reynolds number based on the length of plate for flat plate test cases.

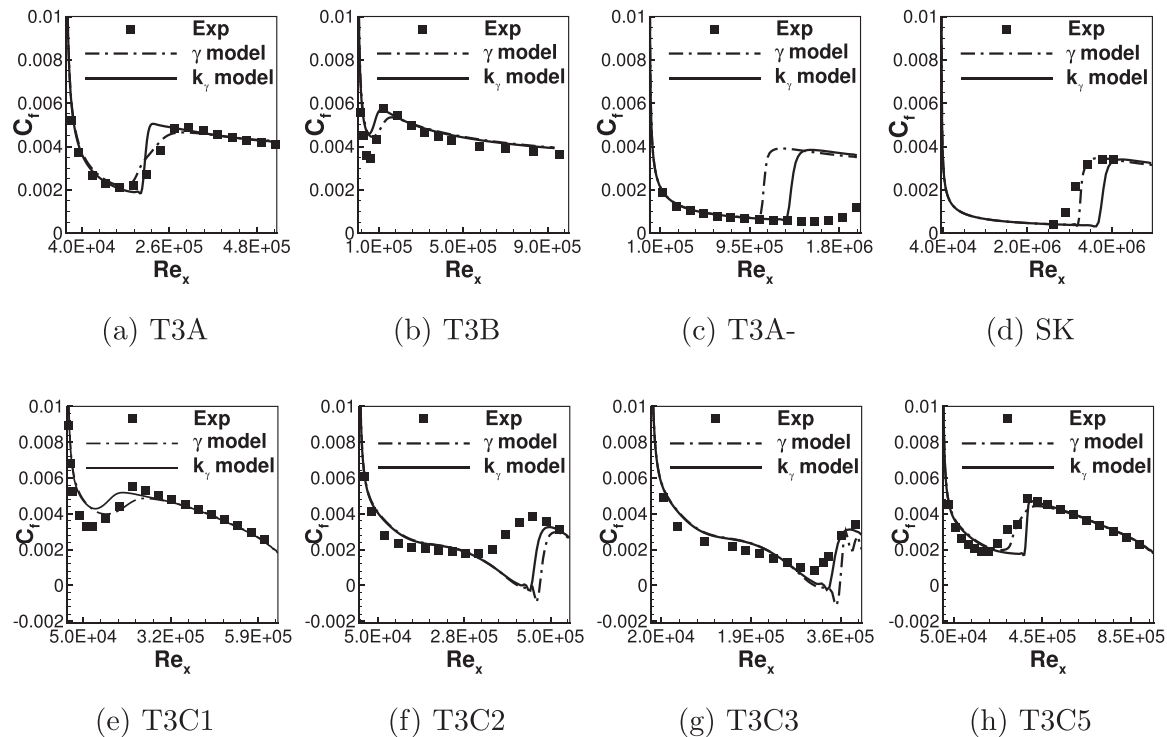


Fig. 9. Skin friction coefficient for flat plate test cases [44].

Fig. 9 compares experimental data [44] for the local skin-friction coefficient along the length of the plate with results obtained using the one-equation γ transition model (dash-dot line) and zero-equation k_γ model (solid line), for flat plate test cases without pressure gradient and with pressure gradient. It can be observed from the skin friction plot for all the flat plate test cases

that although the new zero-equation k_γ model predicts a reasonably accurate transition similar to the one-equation γ model, the length of transition in most of the test cases is short. As seen in the results for the T3A test case, shown in Fig. 9a, the zero-equation k_γ model produces sharper transition as compared to the one-equation γ transition model. Similar results can also be seen

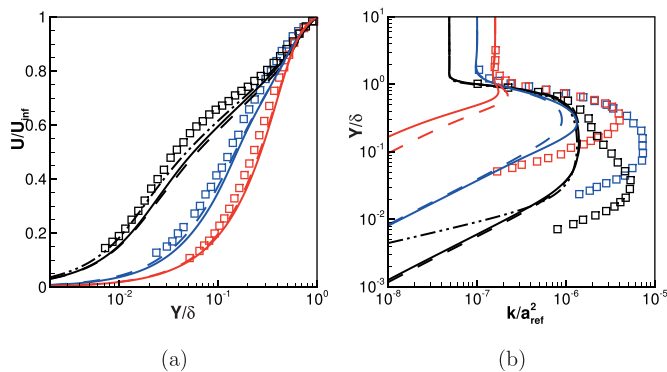


Fig. 10. (a) Velocity and (b) turbulent kinetic energy profiles for T3A test case at laminar (red), transition (blue), and fully turbulent region (black); k_γ model (—), γ model (---), SST2003 model (-.-.-), and experimental data (\square) [44]. (For interpretation of the references to color in this figure legend, the reader is referred to the electronic version of this article.)

in the plot for the test case T3B (Fig. 9b) and the test case with favorable pressure gradient, T3C5 (Fig. 9). It is worthwhile to note that the one-equation γ transition model, itself, predicts sharper transition compared to the two-equation $\gamma - Re_\theta$ model [19] as reported in Menter et al. [27], and the new zero-equation transition model predicts transition that is sharper than that predicted by the one-equation transition model. Further, the results from the algebraic BC transition model in Cakmakcioglu et al. [31] also show a sharp transition for the same flat plate test cases. It seems, as such, that with reduction in the number of equations used for the prediction of transition, the model tends to produce a sharper transition. Hence, it is difficult to control the length of transition in local correlation-based zero-equation transition model.

For the low turbulence intensity test cases, T3A- and SK test cases shown in Fig. 9c and d respectively, the zero-equation k_γ transition model predicts a delayed onset of transition as compared the one-equation γ transition model.

Fig. 10a and b compare the velocity profile and turbulent kinetic energy profile, respectively, predicted by the k_γ and γ transition models with the experimental data [44] for the T3A test case at three different locations on the plate. The first location is in the laminar region (red) at $Re_x = 10^5$, the second location is experimental transition region (blue) at $Re_x = 2 \times 10^5$ and the third location is in the fully turbulent region (black) at $Re_x = 4.9 \times 10^5$. In the fully turbulent region, results using the SST2003 (fully turbulent flow) model are also shown for comparison. The velocity profile predicted by k_γ and γ model overlaps each other in all regions. However, small deviation from the experimental data for both models can be seen in the post-transition region. As seen in Fig. 10b, the turbulent kinetic energy profile predicted by the both k_γ and γ transition model overlap in all but the laminar region, where both profile still shows the same trend. For both transition models, in the laminar region, turbulent kinetic energy decays quickly to negligible value as opposed to the significant turbulent kinetic energy detected in the experiment. Here, one should note that both the k_γ and γ models are not designed to predict the full physics of the boundary layer in the laminar region. The turbulent kinetic energy profiles predicted by both the transition models in turbulent region, although not comparing very well with the experimental data in the inner part of the boundary layer ($y/\delta < 0.1$), reproduces the behaviour of the SST2003 turbulence model for the most part of the boundary layer at this location. Thus, the k_γ model is able to suppress the turbulent kinetic energy in the laminar region which produces the correct Blasius velocity profile and mimics the behaviour of the one-equation γ transition model in the fully turbulent flow and transition region.

Table 3
Computation time for flat plate test cases.

Case	k_γ Model (Min.)	γ model (Min.)	k_γ/γ
T3A	13.36	14.34	0.93
T3B	19.45	20.31	0.95
T3A-	09.85	09.22	1.06
S&K	26.51	25.46	1.04
T3C1	10.98	11.63	0.94
T3C2	14.46	15.81	0.91
T3C3	19.35	21.63	0.89
T3C5	10.18	08.92	1.14

3.4. Computational effort

To quantify the difference in the computational effort required between k_γ and γ model, we measured the total memory used by the processors, and the time it takes to drive the L2-norm of density residual to 10^{-11} . Simulations were performed with the FEST3D code on a machine with Intel(R) Xeon(R) Gold 6142 processor with 64 CPUs.

Fig. 11 shows the convergence history of density residual with respect to the CPU time for the flat plate test cases. As can be observed from the plots, both the k_γ and γ models show very similar convergence. Since the behaviour of the two models are different, instead of using local time step, which is a function of the solution, a global time step of 10^{-4} s for zero pressure gradient test cases and 2×10^{-4} s for pressure gradient test cases was used for the study.

Table 3 shows the computation times for the k_γ and the γ model for the flat plate test cases. It can be observed from the table that whereas the k_γ model requires less time compared to γ model for a majority of the test cases, the reverse is observed for T3A-, SK, and T3C5 test cases. It can possibly be attributed to the fact that whereas the predicted location of transition for the two models are very similar for the other cases, the k_γ model predicts transition further downstream compared to the γ model for the T3A-, SK, and T3C5 test cases that also results in a delay in the onset of transition as can be observed in Fig. 11c. A delayed transition indicates that the solution would require more (overall) iterations (compared to an early transition) for the development of the turbulent boundary layer, which is expected to result in an increase in computational time.

For all these test cases, we observe $\sim 3\%$ computational memory savings. A point to note is that the savings in memory (and computational time) reported herein are with matrix-free LU-SGS time-integration method and are expected to be higher for a fully implicit time-integration method.

4. Applications

4.1. Aerospatiale A-airfoil

The Aerospatiale A-airfoil has been used for validation of CFD codes over the last two decades. It was designed at Aerospatiale and tested in the ONERA (Office National d'Etudes et de Recherches Aéropatiales) F1 and F2 wind tunnels. The data obtained in the F1 wind tunnel is more appropriate for comparison with the numerical predictions of the skin friction coefficient (C_f) and pressure coefficient (C_p); however, due to the unavailability of the original data file and reference, the experimental data are digitized from the work of W. Hassen [45].

For computations presented here, an O-grid similar to the one used in Hasse [45], with 1025 grid points along the airfoil and 257 grid points in the wall-normal direction, is used. Fig. 12 shows the O-grid (every 5th grid point in both directions is shown for clarity),

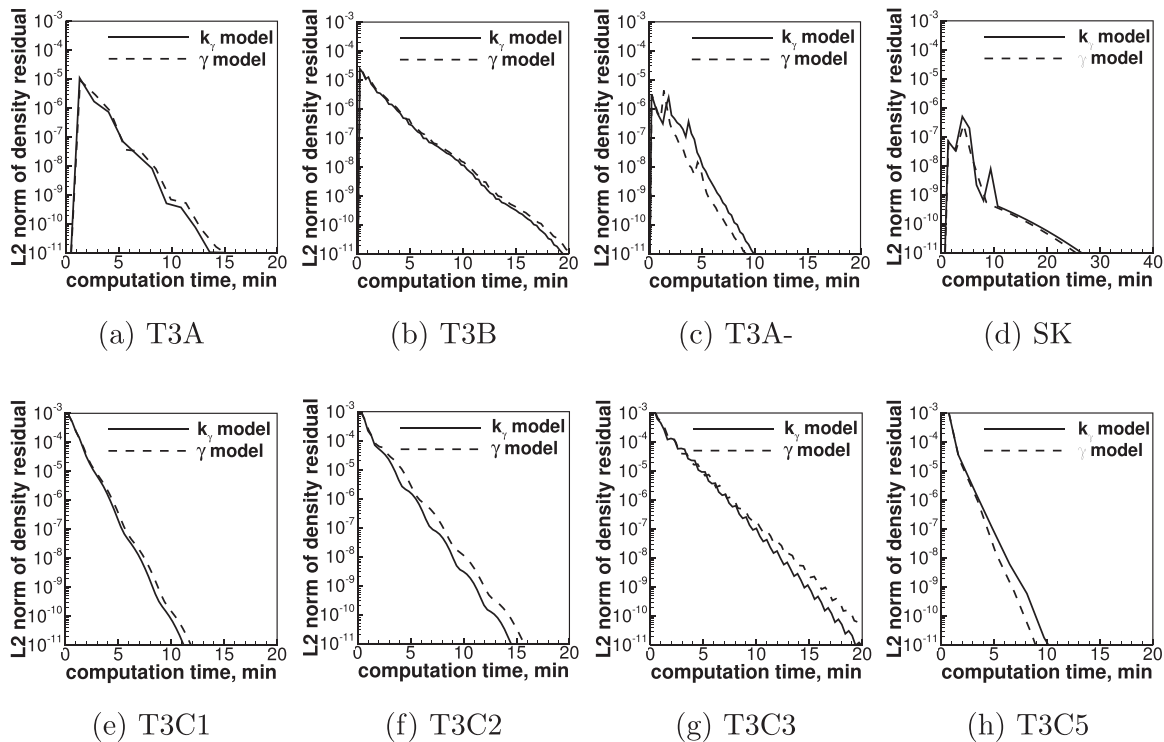


Fig. 11. Residual convergence history.

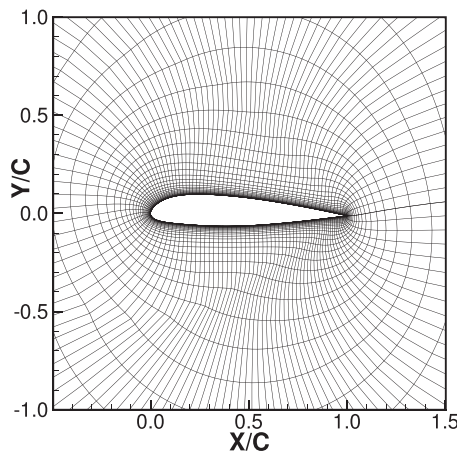


Fig. 12. The O-grid used for the Aerospatiale A-airfoil test case; showing every 5th point in both directions.

with axes normalized with respect to chord length (C), used for the computation.

For flow conditions of 2.1 million Reynolds number, 0.15 Mach number, angle of attack 13.3 degrees and freestream turbulence intensity of 0.05%, the laminar boundary layer over the suction side of the airfoil separates at 12% of the chord length and reattaches as a turbulent boundary layer in the experiment. As shown in the surface pressure coefficient (Fig. 13a) and skin friction coefficient (Fig. 13b) plots, the predictions of the k_γ model practically coincides with that of the one-equation γ model, and both the transition models compare very well with the experimental data. The flow separation on the upper surface of the airfoil, indicated by the negative value of C_f (12% of the chord length), is also captured by both the transition models, as evident from the plot of skin-friction

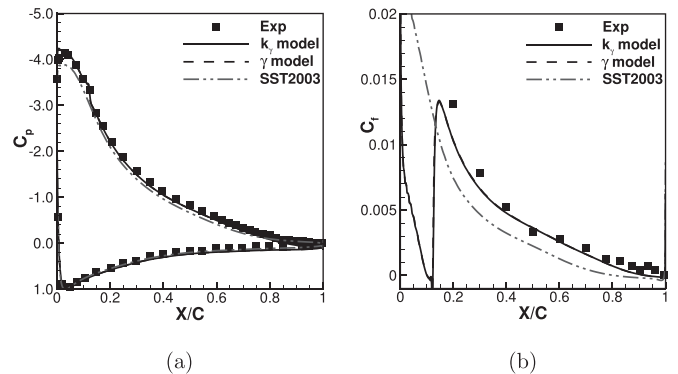


Fig. 13. (a) Pressure coefficient over the Aerospatiale A-airfoil and (b) coefficient of friction on the suction side of Aerospatiale A-airfoil.

in Fig. 13b. The small laminar region before the separation bubble has a pronounced effect on the surface shear-stress after the transition as evident from the difference between the predicted coefficient of friction by either of the transition models and that from the (fully turbulent) SST2003 model; the C_f predictions of the transition model also compare better with experimental data than the predictions of the (fully turbulent) SST2003 model.

The integrated values of lift (C_l) and drag (C_d) coefficients, compared for different grid sizes (h) in Fig. 14, show that the values predicted by the k_γ transition model (and also the one-equation γ model) match the experimental data much better than those predicted by the (fully turbulent) SST2003 model.

4.2. E387 airfoil

McGhee et al. [46] obtained experimental results for flow over Eppler 387 airfoil in the Langley Low-Turbulence Pressure Tunnel

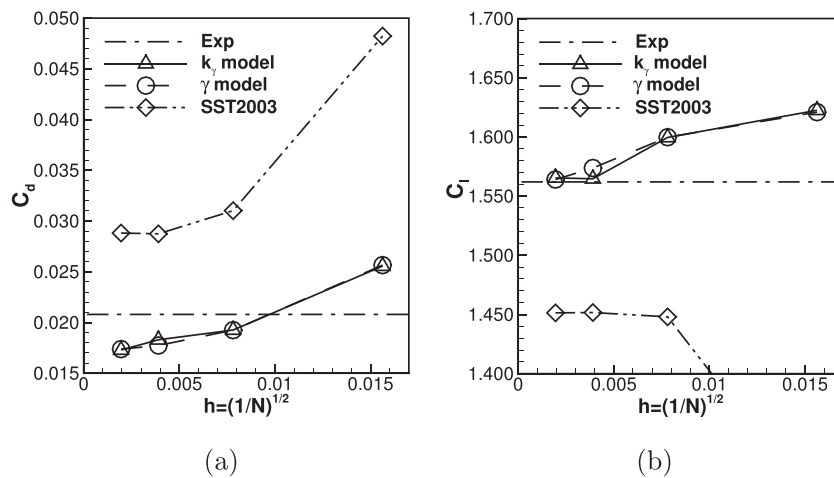


Fig. 14. Comparison of (a) coefficient of drag and (b) coefficient of lift predictions with different grid resolution for Aerospatiale A-airfoil [45].

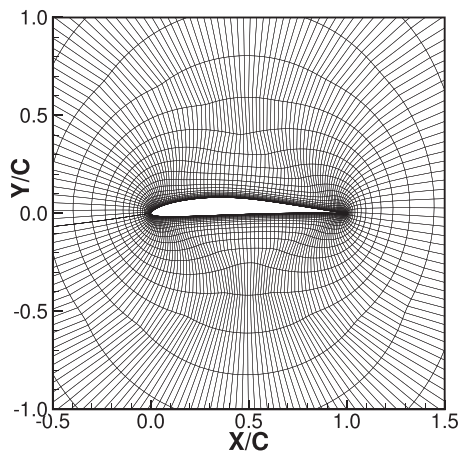


Fig. 15. O-grid used for the E387 airfoil test case; showing every 5th point in both directions.

(LTPT) at Reynolds number of 0.2 million and average freestream turbulence intensity of 0.09%. For the computations, an O-type grid

is used, as shown in Fig. 15. The computational domain consists of 705 grid points along the airfoil, and 180 in the wall-normal direction. The distance of the first (O-type) grid line from the airfoil surface is 10^{-5} m, which keeps the y^+ in the turbulent region below 1.

The computations for the current test case were performed with k_γ transition model, γ transition model, and SST2003 turbulence model. Fig. 16 shows the comparison of these models in terms of drag and lift predictions. As can be seen, both the transition models predict more accurate drag values as compared to the (fully turbulent) SST2003 model. For angles of attack less than the stall value, the lift prediction for k_γ transition model matches with the one equation γ transition model. In the stall region though, the results obtained with k_γ model are closer, at least for the predicted lift values, to the (fully turbulent) SST2003 model, as compared to the one-equation γ transition model. The reason for the discrepancy is not obvious.

In Fig. 17, the pressure coefficient at four different angles of attack: -2° , 0° , 2° and 4° , obtained with k_γ model, is compared with the one-equation γ transition model, (fully turbulent) SST2003 model and experimental data [46]. It can be observed from the experimental C_p data that there is a flow separation on the upper

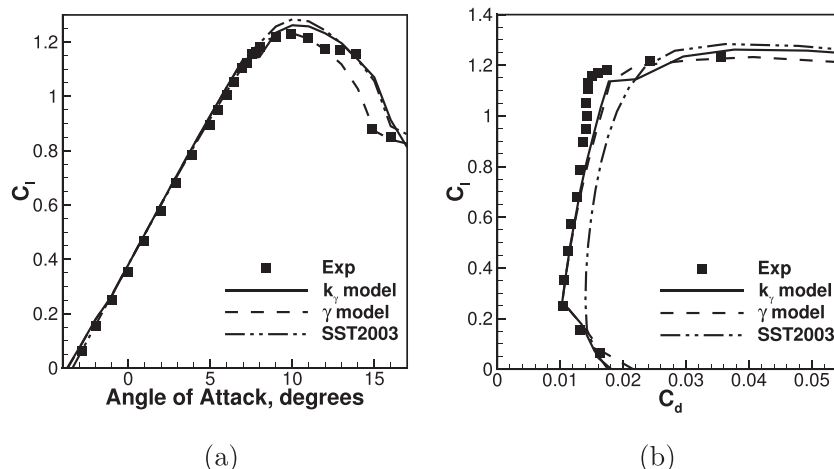


Fig. 16. Comparison of (a) lift coefficient and (b) drag polar for the E387 airfoil test case [46].

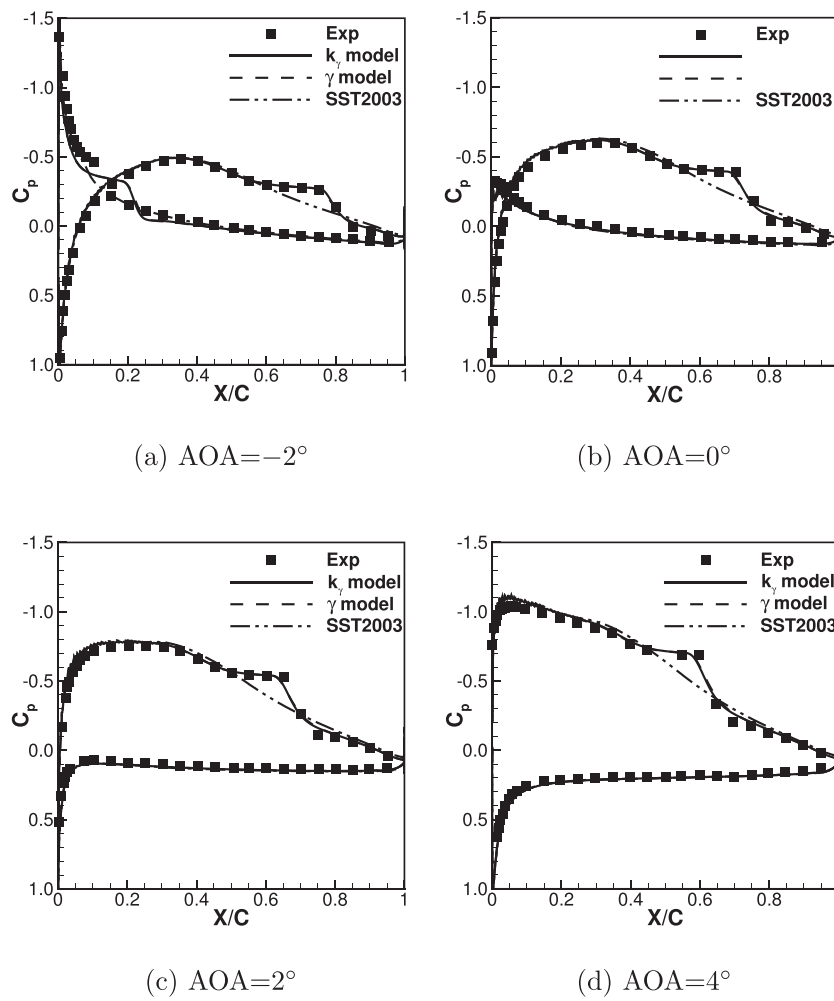


Fig. 17. Pressure coefficient for E387 airfoil test case [46].

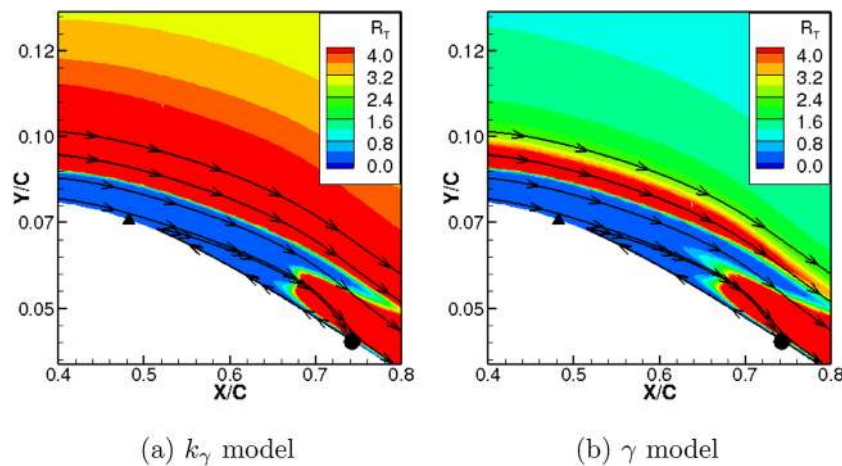


Fig. 18. Flow-separation prediction using k_γ model and γ model for flow past E387 airfoil test case [46].

surface of the airfoil, which is also captured by both the k_γ and the one-equation γ transition models; the fully turbulent flow simulation with the SST2003 model, however, does not capture this.

The flow past the Eppler 387 airfoil at zero angle of attack separates in the laminar regime and reattaches as a fully turbulent boundary layer. Fig. 18 shows the region of flow separation from

the simulations with k_γ and γ transition models. The contours of turbulent Reynolds number (R_T) show that the flow is laminar upstream of separation and reattaches as fully turbulent. The filled triangle and circle on the airfoil surface mark the laminar separation and turbulent reattachment points from the experiment, respectively. As can be observed from the streamlines plotted near

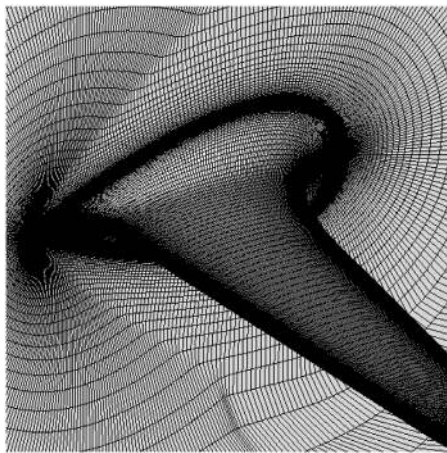


Fig. 19. Grid used for the DLR-F5 test case.

the airfoil surface, the separation bubble obtained from the simulation with k_γ model shows a close match with experimental data in terms of separation length.

4.3. DLR-F5 wing

The three-dimensional DLR-F5 test case consists of a 20° swept wing with 0.65 m span and an average chord length of 0.15 m. The wing was designed with a large fillet at the root section to avoid leading-edge vortex formation. The experiments with this wing were performed by Sobieczky et al. [47] in the DLR wind tunnel, where the wing was mounted on the tunnel’s side-wall. The specific experiment simulated in this work was conducted at a free-stream Mach number of 0.82, turbulence intensity of 0.35%, Reynolds number (based on average chord length) of 1.5 million and angle of attack of 2 degrees.

For the simulations, the wing surface is meshed with 449 grid points in the spanwise direction and 513 grid points along the airfoil. A cuboidal outer domain of 1 m length is used. The wing is mounted on one side, which, along with the wing surface, is treated as a no-slip adiabatic wall while the rest of the domain boundary is treated with far-field boundary condition. The first layer of cells is at a distance of 10^{-7} m from the wall, which results in maximum y^+ of 0.32 over the turbulent region. Fig. 19 shows the mesh on the wing surface and the wall on which it is mounted.

The distribution of the pressure coefficient with chord length at various wing-span locations is shown in Fig. 20. At the section 1.67% from the root of the wing, both of the transition models and turbulence model predict similar results, as shown in Fig. 20a. On the other hand, at the sections 33.854%, 65%, and 80% away from the root of the wing, the fully turbulent flow model (SST2003) shows early shock prediction. The k_γ and γ models predict similar pressure coefficient distribution at wing span locations greater than 50% as seen in the Fig. 20c and d. However, at the wing span location at 33.84% (more correctly between 10 and 50% approximately) from the root, the k_γ model predicts an early transition as compared to the γ transition model, which can be observed in Fig. 20b.

Fig. 21a–c show the surface contours of the coefficient of friction for k_γ , γ , and SST2003 model. The sketch of surface flow features obtained from the experiment, shown in Fig. 21d, is reproduced from [47]. The γ model predicts a separation induced

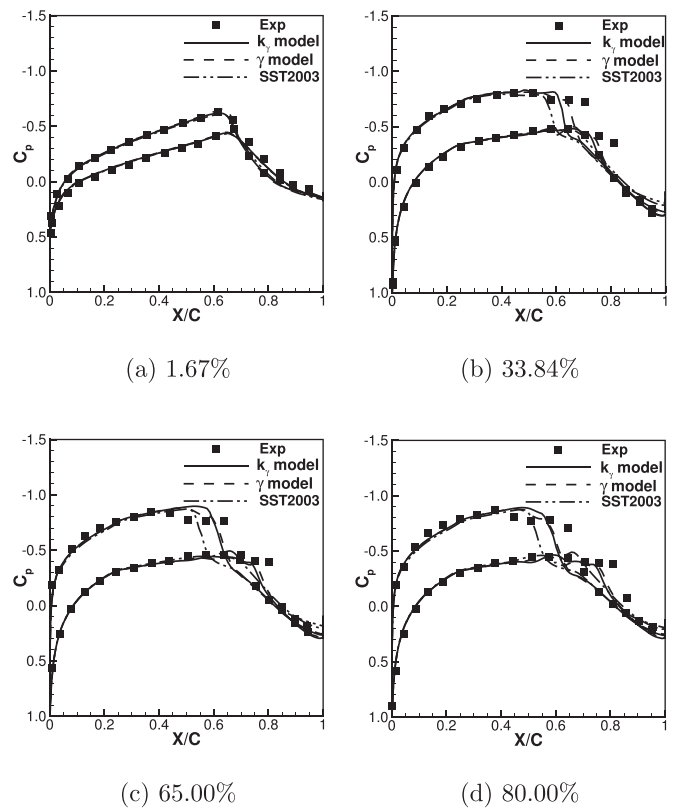


Fig. 20. Comparison of pressure coefficient at various wing span locations (in percentage from root location) obtained for k_γ model, γ model, and SST2003 model with experimental data [47].

Table 4

Computation time for the different test cases in Section 4.

Case	Angle of attack	k_γ Model (hr)	γ model (hr)	k_γ/γ
AA	13.3°	6.75	7.13	0.94
E387	-1°	0.55	0.60	0.93
	1°	0.54	0.57	0.94
	3°	0.56	0.59	0.94
	5°	0.56	0.60	0.94
DLR-F5 ²	2°	128.49	149.05	0.86

² local time step is used in this case.

transition over the whole span of the wing, as seen in Fig. 21b, whereas the k_γ model predicts separation induced transition for the outer half of the wing span and natural transition for the inner half, as seen in Fig. 21a. A point to note is that the correlation used, Eq. (29), does not include effects of crossflow. By introducing crossflow effects [57,58], the γ and k_γ models are expected to produce transition prediction, which compare better with experimentally observed behavior in the inner-half of the wing span.

Similar to the flat plate validation cases, a computation time study was conducted for the test cases in Section 4 on the same machine. The study was conducted with a global time step of 10^{-5} s for Aerospaceal-A airfoil and 5×10^{-5} s for E387 airfoil. Due to a limit of the order of 10^{-12} s on the maximum permissible global time step, the computational time study for the DLR-F5 test was conducted with local time-stepping. As reported in Table 4, the k_γ model shows at least 6% savings in computation time over the γ model.

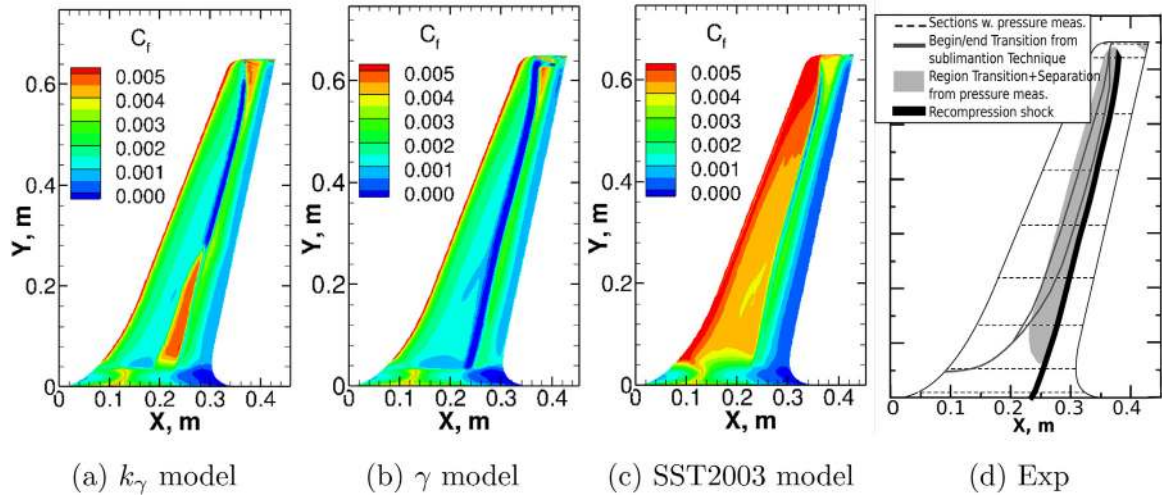


Fig. 21. Comparison of wall shear stress on the surface of DLR-F5 wing [47].

5. Conclusion

A zero-equation local correlation-based transition model, coined as the k_γ model, has been presented in this work. The model derives from a one-equation transition model that solves the transport equation of intermittency and blends this with a two-equation turbulence model through the introduction of a new variable: k_γ . This process results in the modification of the transport equation of k with the addition of new source terms, which are then modeled suitably. As the new model avoids an additional transport equation for intermittency, it can be easily implemented in existing RANS codes with reduced computational memory requirement (compared to one-equation or two-equation transition models), which makes it an attractive option.

The model is validated against a series of standard flat plate - with and without pressure gradient - and airfoil test cases from the literature. The new model is capable of predicting both natural and by-pass transition, and also captures laminar flow separation in airfoils and its reattachment as turbulent boundary layers. Further, the k_γ model produces results similar to the one-equation γ model (albeit with a sharper transition) and provides faster convergence in cases where the predicted transition locations are similar. Comparison of skin-friction contours and pressure-coefficient distribution (at different spanwise locations) predicted by the k_γ model with experimental data for transonic flow past a DLR-F5 swept wing at 2 degrees angle of attack indicate that the k_γ model predicts the flow transition with improved accuracy as one moves away from the wing root.

In summary, it can be said that a novel framework for the construction of non-algebraic local correlation-based zero-equation transition models is presented in this work that can be computationally cheaper and easier to implement compared to existing 1-eqn / 2-eqn models and paves the way for subsequent efforts in this direction.

Declaration of Competing Interest

The authors declare that they have no conflict of interest.

Acknowledgements

The computations were performed in part on the high-performance computing facility at Indian Institute of Technology Madras.

Appendix A. Derivation of source and diffusion terms

Grouping production, destruction and diffusion terms in Eq. (9), we can write:

$$\frac{\partial(\rho k_\gamma)}{\partial t} + \frac{\partial(u_j \rho k_\gamma)}{\partial x_j} = P_{k_\gamma} + P_{k_\gamma}^{lim} - E_{k_\gamma} + D_{k_\gamma} \quad (A.1)$$

Production term The production term in Eq. (A.1) is given by

$$P_{k_\gamma} = \gamma P_k + k P_\gamma \quad (A.2)$$

$$= \gamma(\gamma \mu_t S \Omega) + k(F_{length} \rho S \gamma (1 - \gamma) F_{onset}) \quad (A.3)$$

Substituting the definition of μ_t from Eq. (7)

$$P_{k_\gamma} = \gamma \frac{\gamma \rho a_1 k}{\max(a_1 \omega, S F_2)} S \Omega + k F_{length} \rho S \gamma (1 - \gamma) F_{onset} \quad (A.4)$$

Grouping k and γ terms together to form the k_γ variable we get,

$$P_{k_\gamma} = \left[\frac{\gamma \rho a_1 k_\gamma}{\max(a_1 \omega, S F_2)} S \Omega \right] + \left[F_{length} \rho S k_\gamma (1 - \gamma) F_{onset} \right] \quad (A.5)$$

The first term in production equation looks similar to the production term of k equation, and we term it $P_{k_\gamma}^{(k)}$; the second term is the contribution of the intermittency equation, and we term it $P_{k_\gamma}^{(\gamma)}$. Thus,

$$P_{k_\gamma} = P_{k_\gamma}^{(k)} + P_{k_\gamma}^{(\gamma)} \quad (A.6)$$

where,

$$P_{k_\gamma}^{(k)} = \frac{\gamma \rho a_1 k_\gamma}{\max(a_1 \omega, S F_2)} S \Omega = \gamma \tilde{\mu}_t S \Omega \quad (A.7)$$

where,

$$\tilde{\mu}_t = \frac{\rho a_1 k_\gamma}{\max(a_1 \omega, S F_2)} \quad (A.8)$$

and

$$P_{k_\gamma}^{(\gamma)} = F_{length} \rho S (1 - \gamma) F_{onset} k_\gamma \quad (A.9)$$

A similar derivation yields $P_{k_\gamma}^{lim} = \gamma P_k^{lim}$ for the additional production term in the k -equation.

Destruction term The destruction term in Eq. (A.1) is given by

$$E_{k_\gamma} = \gamma E_k + k E_\gamma \quad (A.10)$$

$$= \gamma [\max(\gamma, 0.1)\beta^* \rho \omega k] + k[C_{a2}\rho\Omega F_{turb}(C_{e2}\gamma - 1)] \quad (A.11)$$

Again, similar to the production term formulation, grouping k and γ terms together to form the k_γ variable, we get

$$E_{k_\gamma} = [\max(\gamma, 0.1)\beta^* \rho \omega k_\gamma] + [C_{a2}\rho\Omega F_{turb}(C_{e2}\gamma - 1)k_\gamma] \quad (A.12)$$

The first term in destruction equation looks similar to the destruction term of k equation, and we term it $E_{k_\gamma}^{(k)}$; the second term is the contribution of the intermittency equation, and we term it $E_{k_\gamma}^{(\gamma)}$. Thus,

$$E_{k_\gamma} = E_{k_\gamma}^{(k)} + E_{k_\gamma}^{(\gamma)} \quad (A.13)$$

where,

$$E_{k_\gamma}^{(k)} = \max(\gamma, 0.1)\beta^* \rho \omega k_\gamma \quad (A.14)$$

and

$$E_{k_\gamma}^{(\gamma)} = C_{a2}\rho\Omega F_{turb}(C_{e2}\gamma - 1)k_\gamma \quad (A.15)$$

Diffusion term The diffusion term in Eq. (A.1) is given by

$$D_{k_\gamma} = \gamma \left(\frac{\partial}{\partial x_j} \left[(\mu + \sigma_k \mu_t) \frac{\partial k}{\partial x_j} \right] \right) + k \left(\frac{\partial}{\partial x_j} \left[(\mu + \sigma_\gamma \mu_t) \frac{\partial \gamma}{\partial x_j} \right] \right) \quad (A.16)$$

Here the following simplifying assumption is made:

$$\sigma_\gamma = \sigma_k$$

and we also define an effective viscosity

$$\mu_{eff} = \mu + \sigma_k \tilde{\mu}_t$$

The diffusion term is then written as

$$D_{k_\gamma} = \gamma \left(\frac{\partial}{\partial x_j} \left[\mu_{eff} \frac{\partial k}{\partial x_j} \right] \right) + k \left(\frac{\partial}{\partial x_j} \left[\mu_{eff} \frac{\partial \gamma}{\partial x_j} \right] \right) \quad (A.17)$$

Using simple product rule of differentiation, Eq. (A.17) is written as

$$D_{k_\gamma} = \frac{\partial}{\partial x_j} \left[\mu_{eff} \gamma \frac{\partial k}{\partial x_j} \right] - \mu_{eff} \frac{\partial k}{\partial x_j} \frac{\partial \gamma}{\partial x_j} + \frac{\partial}{\partial x_j} \left[\mu_{eff} k \frac{\partial \gamma}{\partial x_j} \right] - \mu_{eff} \frac{\partial \gamma}{\partial x_j} \frac{\partial k}{\partial x_j} \quad (A.18)$$

Grouping k and γ terms together to form k_γ variable, we get

$$D_{k_\gamma} = \frac{\partial}{\partial x_j} \left[\mu_{eff} \frac{\partial k_\gamma}{\partial x_j} \right] - 2\mu_{eff} \frac{\partial k}{\partial x_j} \frac{\partial \gamma}{\partial x_j} \quad (A.19)$$

The first term in the diffusion equation looks similar to the diffusion term of k equation, and we term it $D_{k_\gamma}^{(k)}$. Although the second term does not have contribution solely from the intermittency equation, we still term it $D_{k_\gamma}^{(\gamma)}$. Thus,

$$D_{k_\gamma} = D_{k_\gamma}^{(k)} + D_{k_\gamma}^{(\gamma)} \quad (A.20)$$

where,

$$D_{k_\gamma}^{(k)} = \frac{\partial}{\partial x_j} \left[\mu_{eff} \frac{\partial k_\gamma}{\partial x_j} \right] \quad (A.21)$$

and

$$D_{k_\gamma}^{(\gamma)} = -2\mu_{eff} \frac{\partial k}{\partial x_j} \frac{\partial \gamma}{\partial x_j} \quad (A.22)$$

Appendix B. $\tilde{\gamma}$ function

As the estimated intermittency, $\tilde{\gamma}$, is a function of R_T , it is possible that it affects the transition location based on the flow initialization used. As the model presented in the paper is calibrated for freestream initialization, using a fully turbulent or laminar flow initialization may change the transition location, especially for the high-Reynolds number and low-turbulence intensity cases. Fig. B.22 shows the effect of using different initial conditions

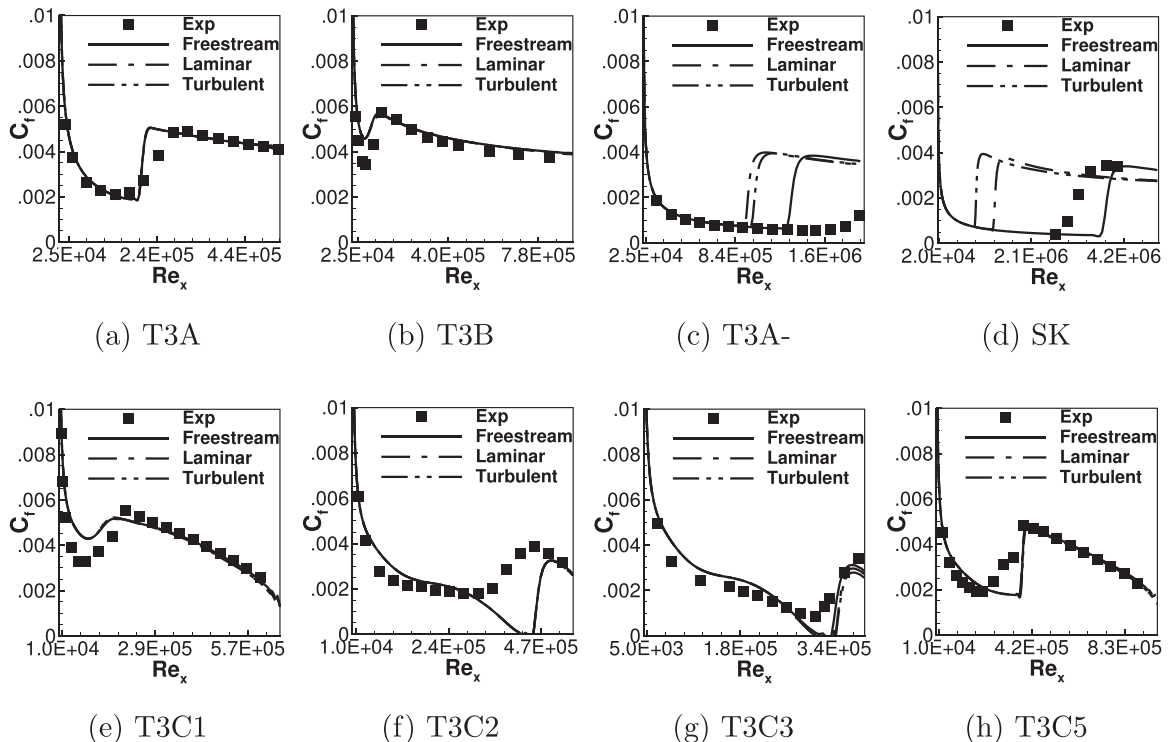


Fig. B.22. The effect of different initial conditions on the prediction of transition local by k_γ model.

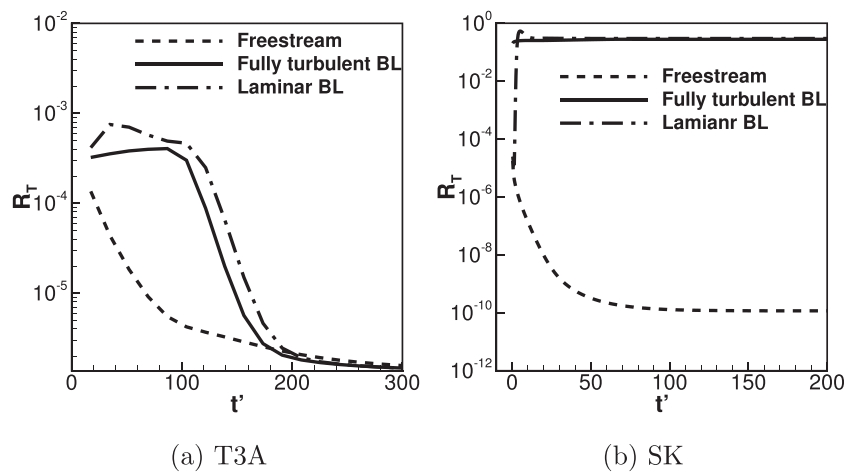


Fig. B.23. Time-evolution of R_T with different initial conditions for (a) T3A flat plate test case at $x = 0.33$ m and $y = 4 \times 10^{-5}$ m, and (b) SK flat plate test case at $x = 0.5928$ m and $y = 4 \times 10^{-5}$ m.

on the transition location for all the flat plate validation test cases presented in this study. All the flat plate test cases with pressure gradient (T3C series), T3A, and T3B test cases show no effect of initial condition on the transition location. However, the T3A- and SK test cases, which are both high Reynolds number and low turbulence intensity cases, show significant early transition when a fully turbulent or laminar boundary layer is used as an initial condition. This is an apparent deficiency in the proposed model, which arises due to the use of R_T in Eq. (16) to model intermittency.

Fig. B.23 shows the evolution of R_T for high-turbulence intensity (T3A) and low-turbulence intensity (SK) test cases with non-dimensional time (t') that is obtained by normalizing t with (L_{ref}/a_{ref}) . Fig. B.23a shows the time-evolution of R_T with freestream, laminar boundary layer, and fully turbulent boundary layer as initial conditions, at a probe location of $x = 0.33$ m and $y = 4 \times 10^{-5}$ m for the T3A flat plate test case. As seen from the plot, the order of the initial R_T is the same with different initial conditions and produces similar (steady state) behavior in the approximated intermittency $\tilde{\gamma}$. In contrast, for the SK test case, shown in Fig. B.23b, the initial values of R_T , at a probe location of $x = 0.5928$ m and $y = 4 \times 10^{-5}$ m, are of different order for different initial conditions, producing completely different (steady state) behavior of approximated intermittency ($\tilde{\gamma}$) with different initial conditions.

References

- Abu-Ghannam BJ, Shaw R. Natural transition of boundary layers the effects of turbulence, pressure gradient, and flow history. *J Mech Eng Sci* 1980;22(5):213–28. doi:10.1243/JMES_JOUR_1980_022_043_02.
- Fransson JHM, Matsubara M, Alfredsson PH. Transition induced by free-stream turbulence. *J Fluid Mech* 2005;527:1–25. doi:10.1017/S0022112004002770.
- Menter FR, Langtry RB, Likki S, Suzen Y, Huang P, Völker S. A correlation-based transition model using local variables part I: model formulation. *J Turbomach* 2006;128(3):413–22. doi:10.1115/1.2184352.
- Mandal AC, Venkatakrishnan L, Dey J. A study on boundary-layer transition induced by free-stream turbulence. *J Fluid Mech* 2010;660:114–46. doi:10.1017/S0022112010002600.
- Simoni D, Lengani D, Dellacasagrande M, Kubacki S, Dick E. An accurate data base on laminar-to-turbulent transition in variable pressure gradient flows. *Int J Heat Fluid Flow* 2019;77:84–97. doi:10.1016/j.ijheatfluidflow.2019.02.008.
- Schlichting H, Gersten K. *Boundary-layer theory*. Springer; 1974. doi:10.1007/978-3-662-52919-5. 978-3-663-52917-1
- Morkovin MV. On the many faces of transition. In: *Viscous drag reduction*. Springer; 1969. p. 1–31. doi:10.1007/978-1-4899-5579-1_1.
- Mayle RE. The 1991 IGTI scholar lecture: the role of laminar-turbulent transition in gas turbine engines. *J Turbomach* 1991;113(4):509. doi:10.1115/1.2929110.
- Van Ingen J. A suggested semi-empirical method for the calculation of the boundary layer transition region. *Tech. Rep.*. Netherland: Delft University of Technology; 1956.
- Smith A, Gamberoni N. *Transition, pressure gradient, and stability theory*. *Tech. Rep.*. Douglas Aircraft Co. ES. 26388; 1956.
- Jones W, Launder B. The calculation of low-Reynolds-number phenomena with a two-equation model of turbulence. *Int J Heat Mass Transf* 1973;16(6):1119–30. doi:10.1016/0017-9310(73)90125-7.
- Durbin PA, Jacobs RG, Wu X. DNS of bypass transition. In: *Closure strategies for turbulent and transitional flows*. Cambridge University Press; 2002. p. 449–63. ISBN 978-0-521-79208-0. doi:10.1017/CBO9780511755385.018.
- Michelassi V, Wissink J, Rodi W. Analysis of DNS and LES of flow in a low pressure turbine cascade with incoming wakes and comparison with experiments. *Flow Turbul Combust* 2002;69(3–4):295–330. doi:10.1023/A:1027334303200.
- Mayle RE. The role of laminar-turbulent transition in gas turbine engines. *J Turbomach* 1993;115(2):207. doi:10.1115/1.2929110.
- Steelant J, Dick E. Modeling of laminar-turbulent transition for high freestream turbulence. *J Fluids Eng* 2001;123(1):22–30.
- Suzen YB, Huang P, Hultgren LS, Ashpis DE. Predictions of separated and transitional boundary layers under low-pressure turbine airfoil conditions using an intermittency transport equation. *J Turbomach* 2003;125(3):455–64. doi:10.1115/1.1580159.
- Bernardos L, Richez F, Gleize V, Gerolymos GA. Algebraic nonlocal transition modeling of laminar separation bubbles using $k-\omega$ turbulence models. *AIAA J* 2019;57(2):553–65. doi:10.2514/1.J057734.
- Dellacasagrande M, Guida R, Lengani D, Simoni D, Ubaldi M, Zunino P. Correlations for the prediction of intermittency and turbulent spot production rate in separated flows. *J Turbomach* 2019;141(3). doi:10.1115/1.4042066.
- Langtry RB, Menter FR. Correlation-based transition modeling for unstructured parallelized computational fluid dynamics codes. *AIAA J* 2009;47(12):2894–906. doi:10.2514/1.42362.
- Lorini M, Bassi F, Colombo A, Ghidoni A. High-order implementation of a non-local transition model in a DG solver for turbomachinery applications. *Comput Fluids* 2016;127:115–30. doi:10.1016/j.compfluid.2015.12.009.
- Menter F, Esch T, Kubacki S. Transition modelling based on local variables. *Eng Turbul Model Exp* 2002;5:555–64. doi:10.1016/B978-008044114-6/50053-3.
- Blumer CB, Van Driest ER. Boundary layer transition- freestream turbulence and pressure gradient effects. *AIAA J* 1963;1(6):1303–6. doi:10.2514/3.1784.
- Menter FR, Langtry R, Völker S. Transition modelling for general purpose CFD codes. *Flow Turbul Combust* 2006;77(1):277–303. doi:10.1007/s10494-006-9047-1.
- Langtry R, Menter F. Transition modeling for general CFD applications in aeronautics. In: *43rd AIAA aerospace sciences meeting and exhibit*. Nevada: Reno; 2005. p. 522. doi:10.2514/6.2005-522.
- Langtry RB, Menter F, Likki S, Suzen Y, Huang P, Völker S. A correlation-based transition model using local variables part II: test cases and industrial applications. *J Turbomach* 2006;128(3):423–34. doi:10.1115/1.2184353.
- Kelterer ME, Pecnik R, Sanz W. Computation of laminar-turbulent transition in turbomachinery using the correlation based γ - $re\theta$ transition model. In: *Turbo expo: power for land, sea, and air*; 2010. p. 613–22.
- Menter FR, Smirnov PE, Liu T, Avancha R. A one-equation local correlation-based transition model. *Flow Turbul Combust* 2015;95(4):583–619. doi:10.1007/s10494-015-9622-4.
- Coder J.G., Maughmer M.D.. One-equation transition closure for eddy-viscosity turbulence models in CFD. *AIAA paper* 2012-0672 (January):1–15. doi:10.2514/6.2012-672.

- [29] Ge X, Arolla S, Durbin P. A bypass transition model based on the intermittency function. *Flow Turbul Combust* 2014;93(1):37–61. doi:10.1007/s10494-014-9533-9.
- [30] Bas O, Cakmakcioglu SC, Kaynak U. A novel intermittency distribution based transition model for low-re number airfoils. In: 31st AIAA applied aerodynamics conference. Reston, Virginia: American Institute of Aeronautics and Astronautics; 2013. p. 1–13. doi:10.2514/6.2013-2531.
- [31] Cakmakcioglu SC, Bas O, Kaynak U. A correlation-based algebraic transition model. *Proc Inst Mech Eng Part C* 2017;0(0). doi:10.1177/0954406217743537.
- [32] Spalart P, Allmaras S. A one-equation turbulence model for aerodynamic flows. 30th aerospace sciences meeting and exhibit. Reston, Virginia: American Institute of Aeronautics and Astronautics; 1992 January. doi:10.2514/6.1992-439.
- [33] JACOBS RG, DURBIN PA. Simulations of bypass transition. *J Fluid Mech* 2001;428:185–212. doi:10.1017/S0022112000002469.
- [34] Walters DK, Cokljat D. A three-equation eddy-viscosity model for Reynolds-averaged Navier Stokes simulations of transitional flow. *J Fluids Eng* 2008;130(12):121401. doi:10.1115/1.2979230.
- [35] Pacciani R, Marconcini M, Fadaei-Ghotbi A, Lardeau S, Leschziner MA. Calculation of high-lift cascades in low pressure turbine conditions using a three-equation model. *J Turbomach* 2011;133(3):031016. doi:10.1115/1.4001237.
- [36] Lopez M, Keith Walters D. A recommended correction to the $kT - kL - \omega$ transition-sensitive eddy-viscosity model. *J Fluids Eng* 2016;139(2):024501. doi:10.1115/1.4034875.
- [37] Juntasaro E, Ngiamsoongnirn K. A new physics-based γkL transition model. *Int J Comput Fluid Dyn* 2014;28(5):204–18. doi:10.1080/10618562.2014.921681.
- [38] Kubacki S, Dick E. An algebraic model for bypass transition in turbomachinery boundary layer flows. *Int J Heat Fluid Flow* 2016;58:68–83. doi:10.1016/j.ijheatfluidflow.2016.01.001.
- [39] Kubacki S, Dick E. An algebraic intermittency model for bypass, separation-induced and wake-induced transition. *Int J Heat Fluid Flow* 2016;62:344–61. doi:10.1016/j.ijheatfluidflow.2016.09.013.
- [40] Mishra A, Kumar G, De A. Prediction of separation induced transition on thick airfoil using non-linear URANS based turbulence model. *J Mech Sci Technol* 2019;33(5):2169–80. doi:10.1007/s12206-019-0419-6.
- [41] Menter FR. Eddy viscosity transport equations and their relation to the $k - \epsilon$ model. *J Fluids Eng* 1997;119(4):876–84. doi:10.1115/1.2819511.
- [42] Menter FR, Kuntz M, Langtry R. Ten years of industrial experience with the SST turbulence model. *Turbul Heat Mass Transf* 2003;4(1):625–32.
- [43] Schaubauer G, Klebanoff P. Contributions on the mechanics of boundary-layer transition. *Tech. Rep.*. Washington, DC, United States: National Bureau of Standards; 1956.
- [44] Savill A. Some recent progress in the turbulence modelling of by-pass transition. In: So RMC, Speziale CG, Launder BE, editors. Near-wall turbulent flows. New York: Elsevier; 1993. p. 829–48.
- [45] Hasse W. Chapter 18 in part IV: the aerospaciale a-airfoil. In: Werner H, Aupoix B, Bunge U, Schwaborn D, editors. Flowmania - a europea initiative on flow physics modelling. Notes on Numerical Fluid Mechanics, 94. Verlag Berlin Heidelberg: Springer; 2006. p. 367–78. doi:10.1007/978-3-540-39507-2_42.
- [46] Mcghee RJ, Walker BS, Milard BF. Experimental results for the Eppler 387 airfoil at low Reynolds numbers in the Langley low-turbulence pressure tunnel. *Tech. Rep.*. Hampton, VA, United States: NASA Langley Research Center; 1988.
- [47] Sobieczky H. DLR-F5: Test Wing for CFD and Applied Aerodynamics. *Tech. Rep.*. AGARD; 1994.
- [48] Singh Sandhu JP, Girdhar A, Ramakrishnan R, Teja R, Ghosh S. A convergence study of solutions using two two-equation RANS turbulence models on a finite volume solver for structured grids. In: 2018 fluid dynamics conference; 2018. p. 3859. doi:10.2514/6.2018-3859.
- [49] Sandhu JPS, Girdhar A, Ramakrishnan R, Teja R, Ghosh S. FEST-3D: finite-volume explicit structured 3-dimensional solver. *J Open Source Softw* 2020;5(46):1555. doi:10.21105/joss.01555.
- [50] Wilcox D. Effects of compressibility. In: *Turbulence modeling for CFD, 1. DCW Industries; 2006. p. 239–97. ISBN 9781928729082.*
- [51] Van Leer B. Towards the ultimate conservative difference scheme. V. A second-order sequel to Godunov's method. *J Comput Phys* 1979;32(1):101–36. doi:10.1016/0021-9991(77)90095-X.
- [52] Liou M-S. A sequel to AUSM, part II: AUSM+-UP for all speeds. *J Comput Phys* 2006;214(1):137–70. doi:10.1016/j.jcp.2005.09.020.
- [53] Luo H, Baum JD, Löhner R. A fast, matrix-free implicit method for compressible flows on unstructured grids. *J Comput Phys* 1998;146(2):664–90. doi:10.1006/jcph.1998.6076.
- [54] Weiss JM, Smith WA. Preconditioning applied to variable and constant density flows. *AIAA J* 1995;33(11):2050–7. doi:10.2514/3.12946.
- [55] Kitamura K, Shima E, Fujimoto K, Wang ZJ. Performance of low-dissipation euler fluxes and preconditioned LU-SGS at low speeds. *Commun Comput Phys* 2011;10(1):90–119. doi:10.4208/cicp.041109.160910a.
- [56] Suluksna K, Dechaumphai P, Juntasaro E. Correlations for modeling transitional boundary layers under influences of freestream turbulence and pressure gradient. *Int J Heat Fluid Flow* 2009;30(1):66–75. doi:10.1016/j.ijheatfluidflow.2008.09.004.
- [57] Medida S, Baeder J. A new crossflow transition onset criterion for RANS turbulence models. In: 21st AIAA computational fluid dynamics conference; 2013. p. 3081. doi:10.2514/6.2013-3081.
- [58] Grabe C, Krumbein A. Extension of the $\gamma - re\theta t$ model for prediction of cross-flow transition. In: 52nd aerospace sciences meeting; 2014. p. 1269. doi:10.2514/6.2014-1269.